Chapter 1
Optically Injected Single-Mode Quantum Dot Lasers

B. Kelleher, D. Goulding, S. P. Hegarty, G. Huyet, E. A. Viktorov and T. Erneux

Abstract The response of an optically injected quantum dot semiconductor laser is studied both experimentally and theoretically. Specifically, the locking boundaries are investigated, revealing features more commonly associated with Class A lasers rather than conventional Class B semiconductor lasers (SLs). Further, various dynamical regimes are observed including excitability and multistability. Of particular interest is the observation of a phase-locked bistability. We determine the stability diagram analytically using appropriate rate equations for quantum dot lasers. In particular, the saddle-node (SN) and Hopf bifurcations forming the locking boundaries are examined and are shown to reproduce the observed experimental stability features. The generation of the phase-locked bistability is also explained via a combination of these bifurcations.

B. Kelleher (✉) · G. Huyet
Centre for Advanced Photonics and Process Analysis,
Cork Institute of Technology and Tyndall National Institute,
Lee Maltings, Dyke Parade, Cork, Ireland
e-mail: bryan.kelleher@tyndall.ie

D. Goulding · S. P. Hegarty
Tyndall National Institute, University College Cork, Lee Maltings,
Dyke Parade, Cork, Ireland

E. A. Viktorov · T. Erneux
Université Libre de Bruxelles, Optique Nonlinéaire Théorique,
Campus Plaine, Code Postal 231, 1050 Bruxelles, Belgium
e-mail: terneux@ulb.ac.be

Z. M. Wang (ed.), *Quantum Dot Devices*, Lecture Notes in Nanoscale Science and Technology 13, DOI: 10.1007/978-1-4614-3570-9_1,

Introduction

Semiconductor lasers (SLs) have become the optical source of choice in many applications due to their high efficiency, simplicity of modulation, and small size. However, in some applications where it is necessary for the intensity noise level to remain low, they suffer from intensity fluctuations that are enhanced by their inherent relaxation oscillations (ROs). The phenomenon of ROs is familiar in the laser physics community. When a laser is perturbed from its steady-state operation, it does not immediately return to its original position. Instead, the relaxation to the steady state typically occurs in one of two ways known as Class A and Class B behavior. In a Class A laser, the laser approaches the equilibrium exponentially like an overdamped oscillator while in a Class B laser it slowly oscillates back to its stable steady-state like an underdamped oscillator, and these are the aforementioned ROs. Class A lasers include Ar, He–Ne, and dye lasers while Class B lasers include most of the lasers used today such as CO_2, solid state and SLs. When subject to optical injection, Class A and Class B lasers exhibit quite different stability properties. Class B lasers admit a rich number of sustained pulsating intensity regimes which have been studied systematically over the last decade for semiconductor and solid-state lasers (see [24] for a recent review). Class A lasers, free of ROs, are much more stable [20]. Recent efforts to suppress the RO-induced instabilities in conventional SLs have concentrated on increasing the photon lifetime above the carrier lifetime. This can be achieved by increasing either the cavity length or the cavity finesse. The first technique has been successfully applied with a several-meter-long cavity in SLs [3]. The second alternative is technically easier and has been explored using half of a vertical cavity surface emitting laser ($\frac{1}{2}-$ VCSEL) in a short external cavity [4, 5].

The development of the QD laser was a concerted effort to combine the best features of SLs (solid state, electrically injectable, small size) with some of the best features of atomic lasers (narrow gain bandwidths, zero linewidth enhancement factor). In this work we consider both experimentally and theoretically the optical injection of a single-mode [distributed feedback (DFB)] QD laser. QD lasers experiencing optical feedback have demonstrated excellent stability properties [21] and so one might also expect enhanced stability properties for an optically injected QD laser. It is known from previous studies that QD lasers exhibit a certain number of properties that make them attractive for application [6]. A particularly attractive property is an unusually high damping of the ROs [18] in comparison to their bulk and quantum well (QW) counterparts. This high damping has been cited as the principal reason for the increased stability of such devices subject to optical feedback [21], optical injection [8, 10, 14], and mutual coupling [12, 15] configurations. We determine here an experimental stability diagram with the injection strength and the detuning as control parameters and note that it is considerably different from that of a conventional QW laser. In particular, the injected QD laser exhibits stability for arbitrary values of the injection rate provided the detuning is sufficiently low. A region of bistability between two

coexisting fixed points is also possible. While these features were noted in [8], in this work we examine the result in greater depth and the observations are substantiated analytically by studying rate equations appropriate for a QD laser.

Experimental Details

The experiment was carried out on several DFB InAs devices of similar construction to those described in detail in [19]. The devices have a 5-QD-layer structure grown by solid-source molecular beam epitaxy (MBE) and consist of 2.4 InAs monolayers topped with 5 nm GaInAs, stacked in a 200 nm thick optical cavity. A 35 nm GaAs spacer is used between the QD layers and optical confinement is provided by $Al_{0.85}Ga_{0.15}As$ cladding layers. The single-mode ridge waveguide lasers were approximately 2 μm long. The master laser was a commercial external cavity tunable device with linewidth < 100 kHz. It was tunable in steps of 0.1 pm and its output was guided in a polarization maintaining fiber and coupled into the slave waveguide using a lensed fiber via polarization controllers. To prevent undesired feedback, an optical isolator with an isolation greater than 40 dB was used at the output side of the slave. The slave laser was biased at 1.5 times threshold and its output was measured using a number of different diagnostic tools: an optical spectrum analyser; a 12 GHz photodiode, amplified and connected to an electrical spectrum analyzer; and a real-time oscilloscope of 6 GHz bandwidth and a sampling rate of 40 giga-samples per second.

There are three control parameters available experimentally, namely the master power (giving the injection rate) Γ, the slave injection current J, and the detuning Δ, defined as the angular frequency difference between the master and slave lasers. Figure 1.1 shows the evolution of the power spectrum of the slave DFB laser as the detuning is varied at a fixed relatively low injection strength. Both the power of the master and the slave injection current were fixed and the detuning was systematically varied by changing the wavelength of the master laser. At each value of the master wavelength an RF spectrum was recorded and Fig. 1.1 shows a false color plot of the spectra over a wide range of detuning. Clear from this figure are the regions of beating between the master and slave lasers far from zero detuning and a stable locked region in the center. A noteworthy feature is the large area of stable locked operation found for each injection strength tested. In particular, in stark contrast to optically injected QW lasers, stable phase-locked operation was found at zero detuning for each injection strength considered with the QD lasers.

In [10] the optical injection properties of a multimode QD laser were reported. There it was shown that for low to moderate injection strengths, fast dynamics can be observed close to the locking boundary for negative detuning. In the case of a single-mode QD laser dynamical regimes appear close to the locking boundaries for both positive and negative detunings as shown in Fig. 1.1. The nature of these regions depends on the injection strength. We define the injection strength to be the ratio of the intensity of the light injected into the lasing cavity to the intensity of the light in

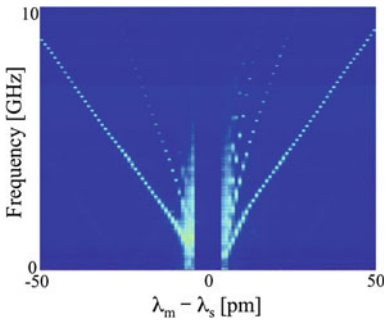

Fig. 1.1 Experimental microwave mask showing fast dynamics near both the positive and negative detuning unlocking boundaries

the cavity when free running. The lowest injection strength in this work was 0.004. For negative detuning and injection strengths up to 0.02, intensity pulses such as those in Fig. 1.2 were observed and for positive detuning and injection strengths up to 0.01, intensity pulses such as those in Fig. 1.3 were observed. These were very rare and apparently randomly spaced initially with a broad power spectrum. As the magnitude of the detuning was increased, they became more frequent, eventually becoming a periodic train of pulses much like a distorted sine curve with the fast/slow characteristic motion of the pulses with a sharply peaked power spectrum. At this point the slave had become unlocked. The shape of the pulses differs depending on the sign of the detuning since there is a nonzero α-factor. For the case of negatively detuned pulses, the intensity drops before rising above the phase-locked intensity and then returns to the steady-state value. For the positively detuned side the intensity increases, then drops below the steady-state value, and eventually again recovers to the steady-state value. These are excitable pulses resulting from 2π phase rotations of the slave electric field as shown in [14]. In [23] complicated multipulse excitability in optically injected QW lasers was predicted and has since been observed in [16]. In contrast to this, for single-mode quantum dot lasers, only single pulse excitability is observed. This has been explained as also resulting from the high RO damping in these devices in [16]. These excitable pulses arise close to the saddle-node (SN) bifurcation similar to the phase slips observed in the Adler model [1]. The logic is as follows. At very low absolute values of the detuning, the stable and unstable points are sufficiently separated to avoid any noise-induced pulsations (that is the noise is not sufficient to push the laser away from the stable point and beyond the unstable threshold point) and as a result quiet regions of locking are observed. As the magnitude of the detuning is increased, the stable and unstable fixed points become progressively closer until eventually noise is sufficient to push the system past the unstable point resulting in a 2π rotation of the electric field and a consequent intensity pulsation. As the magnitude of the detuning is increased even further the pulses occur more and more frequently until eventually the two fixed points collide and annihilate each other leaving a ghost at which point the system's time series becomes a periodic train (modulo noise) with the characteristic shape of the pulses. The dynamical behavior close to the boundaries in the microwave mask shown in Fig. 1.1 consisted of such pulses. In [15] a similar phenomenon was observed in a delayed mutually

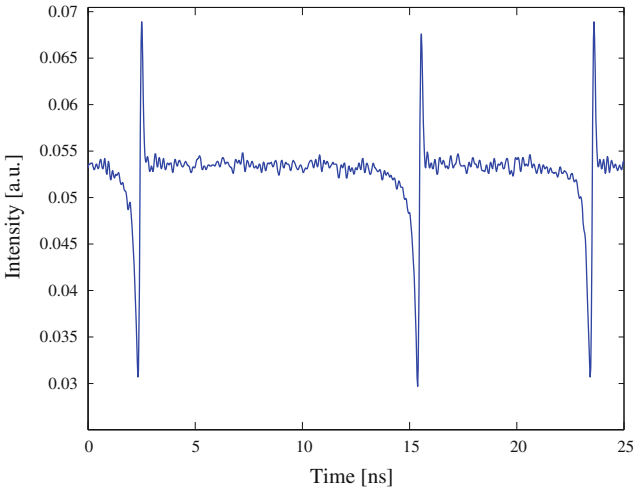

Fig. 1.2 Experimentally obtained intensity pulses for the case of negative detuning

coupled configuration of quantum dot lasers. In this case, due to the delayed mutual coupling, a pulse train is observed rather than individual pulses. As the injection strength is increased the dynamical behavior changes significantly and similar to the multimode case [10], various different dynamical regimes may be observed. The first change is the disappearance of the excitable pulses near the positive detuning unlocking boundary. These are replaced by a noise-induced switching between a stable point and a limit cycle (with a higher average power) as shown in Fig. 1.4. For the same injection power, the slave laser is still undergoing excitable pulsing close to the negatively detuned unlocking boundary, clearly showing again the asymmetry in the dynamical bifurcations in the optically injected laser system due to the nonzero α-factor. If the injection strength is increased further, this switching is replaced by chaotic behavior (Fig. 1.5) and eventually the SN bifurcation disappears and instead locking is via a Hopf bifurcation which results in the slave laser moving directly from unlocked to locked behavior as shown in Fig. 1.6. The proximity of the chaotic behavior to the disappearance of the SN and the appearance of the Hopf suggests strongly that this chaos has an organizing center in a codimension-2- fold-Hopf point at their intersection. The Hopf bifurcation first appears for injection strengths of 0.016. This is higher than that for conventional semiconductor lasers under optical injection but is consistent with measurements of the RO damping rate for quantum-dot-based devices reported in, for example, [17, 21].

At the injection strength where the positively detuned locking boundary changes to a Hopf bifurcation, excitable pulsations are still observed near the negatively detuned boundary. Increasing the injection strength still further the negatively detuned excitable pulses also disappear and are replaced with a bistability between a stable point and a limit cycle (of lower average power) as

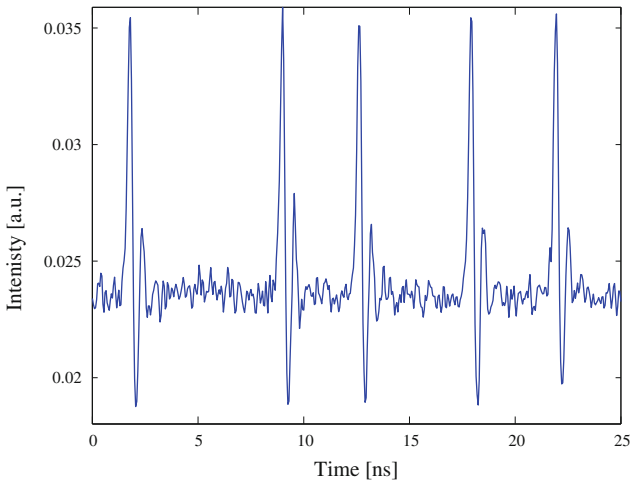

Fig. 1.3 Experimentally obtained intensity pulses for the case of positive detuning in an optically injected QD laser

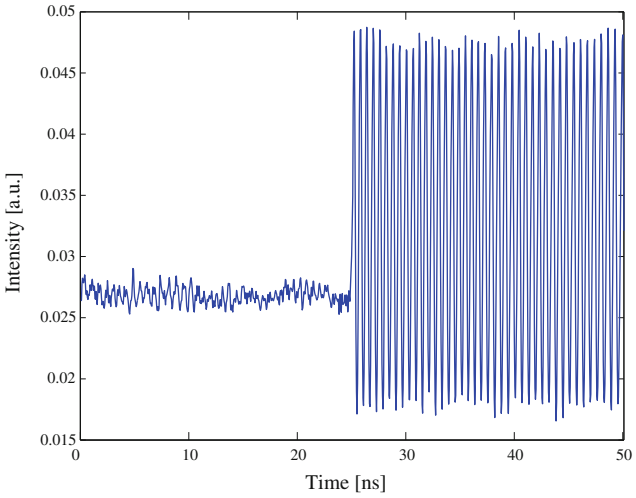

Fig. 1.4 Time trace of switch from stable state to higher average power limit cycle behavior for the case of positive detuning in an optically injected QD laser

shown in Fig. 1.7. This limit cycle undergoes a period doubling bifurcation and the switching is then between this period doubled cycle and the stable point as shown in Fig. 1.8. Finally, there is a region where two phase-locked solutions of different intensities coexist. This is the dynamical behavior of most interest for this work. Figure 1.9 shows an example of a noise-induced switching between the two locked states. The transition between the two steady states is

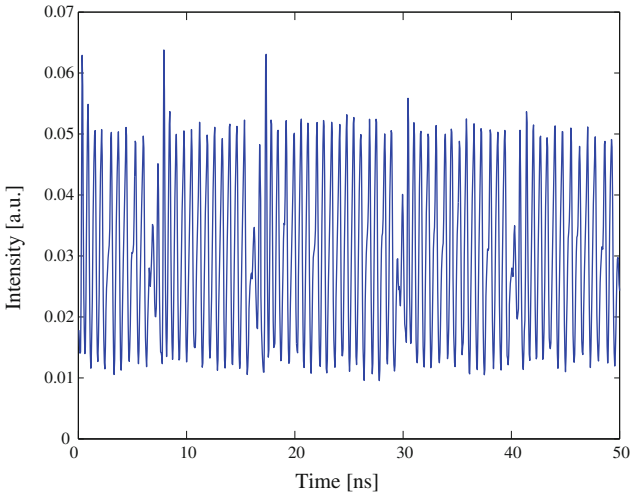

Fig. 1.5 Time trace of chaotic attractor for the case of positive detuning in an optically injected QD laser

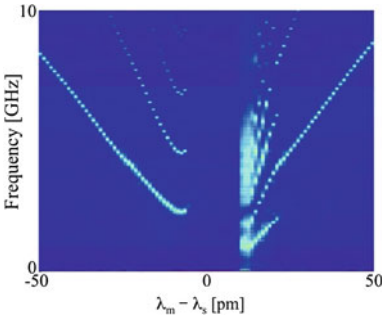

Fig. 1.6 Experimentally obtained power spectra for an optically injected QD DFB laser at a higher injection strength than that in Fig. 1.1. At this injection strength the laser moves directly from unlocked to locked on the positive detuning boundary (lower master wavelength) with no fast dynamical regime. This absence of noise-induced dynamics indicates that the locking is via a Hopf bifurcation rather than via an SN bifurcation

sharp and the relaxation includes only one spiked oscillation. It suggests that the decay of the relaxation dynamics occurs at the same time scale as that of the RO frequency in contrast to the typical Class B laser and thus we speak of the Class A limit. This behavior is not possible for a weakly damped QW laser except very close to threshold. At this injection strength the locking boundary for negative detuning is also a Hopf bifurcation. However, the SN bifurcation has not disappeared but instead lies inside the locking region where it creates the second locked solution.

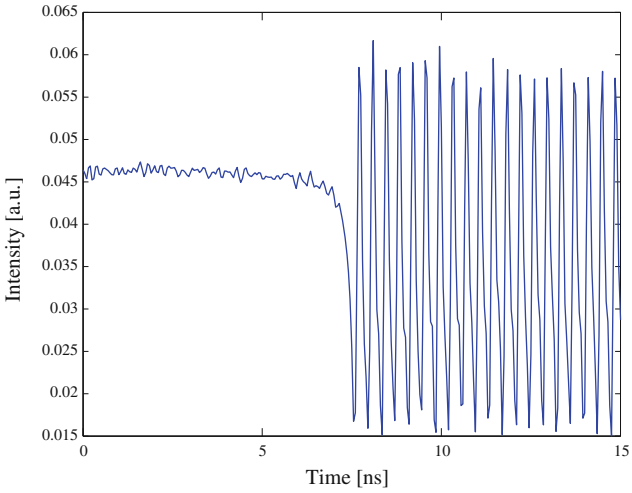

Fig. 1.7 Time trace of switch from stable state to lower average power limit cycle behavior for the case of negative detuning in an optically injected QD laser

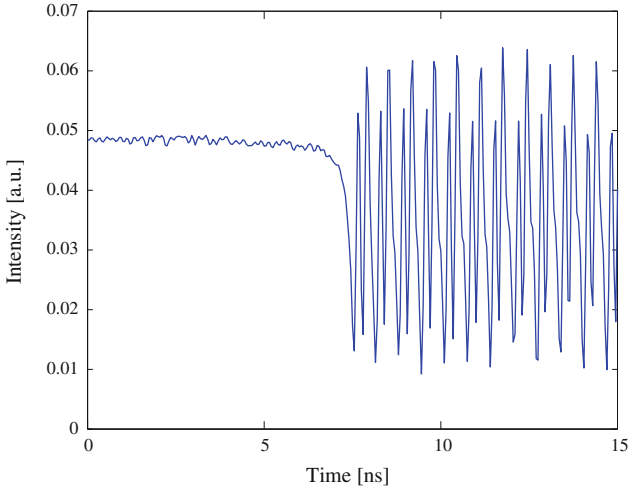

Fig. 1.8 Time trace of switch from stable state to period two limit cycle behavior for the case of negative detuning in an optically injected QD laser

The results of the experimental mapping of the observed dynamics are shown in Fig. 1.10. The black lines mark the SN bifurcations and the red lines mark the Hopf bifurcations. Between the two black lines in the upper left of the figure a phase-locked bistability was observed. A zoom of the low injection strength region is shown in Fig. 1.11 with the various dynamical regimes observed labeled.

There are a number of fundamental differences between the mappings in Figs. 1.10 and 1.11 and the injection dynamics reported in [22] for the conventional

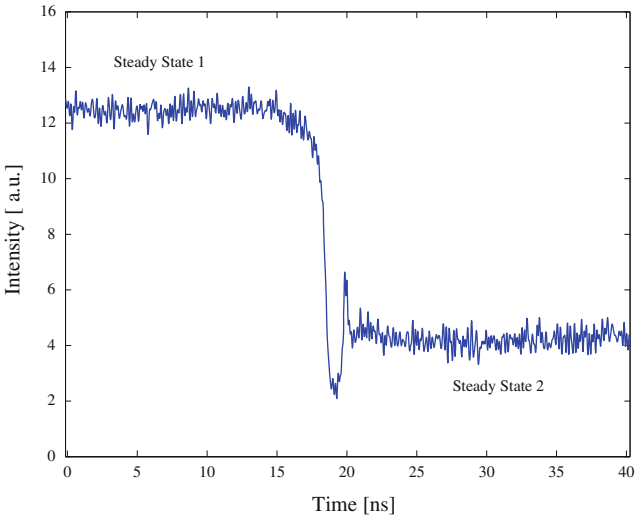

Fig. 1.9 Time trace of switch between two distinct stable phase locked states in an optically injected QD laser

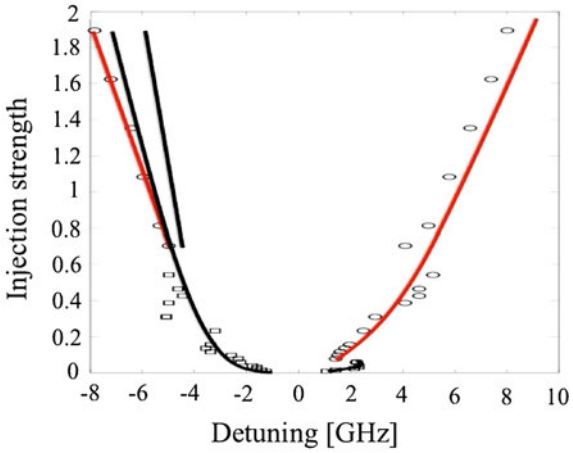

Fig. 1.10 Experimental stability diagram. The injection strength is defined as the power of the light injected into the cavity divided by the power in the cavity when free running. The *circles* and *rectangles* show the experimental points while the lines are added as a guide. The *solid black lines* (through the *rectangles*) are SN bifurcations. The *solid red lines* (through the *ellipses*) are Hopf bifurcations. Between the two *black lines* at the *top left* of the figure a phase-locked bistability is observed

QW laser and reviewed in detail in [24]. Instead, we note a similarity between the stability diagram in Fig. 1.10 and that of a Class A laser [20]. The Hopf bifurcation line differs from that which occurs for an injected QW laser and, in particular, it does not cross the zero detuning line allowing stable phase-locked behavior at zero

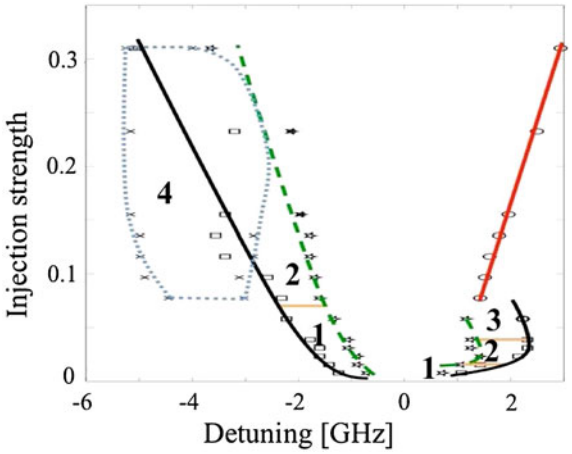

Fig. 1.11 A zoom of the low injection region of the experimental stability diagram. As before, the lines are added as guides. The *solid black lines* (through the *rectangles*) correspond to SN bifurcations and the *solid red* (through the *ellipses*) to Hopf bifurcations. The *dashed green lines* (through the *stars*) are the dynamical boundaries: between these and the *black lines* various different dynamical regimes were observed. The *blue dotted line* (through the x's) marks a period doubling line. The dynamical regions are labeled as 1 through 4. *1* Excitable pulses. *2* Switching between phase-locked behavior and a limit-cycle. *3* Switching between phase-locked behavior and a chaotic attractor. *4* Period doubling. Note that the period doubling can be both inside and outside the locking region. The same is true for the chaotic region although only that portion inside the locking region is shown

detuning for arbitrary injection strengths. Furthermore, as already stated, except very close to the laser threshold [13], the coexistence of two stable locking states is not possible for a QW laser. Also, the extent of the locking via an SN bifurcation for positive detuning is greatly increased as one would expect for a more highly damped slave laser. These observations suggest a significant impact from the nonlinear capture dynamics in QD lasers provided by the Pauli blocking factor. More precisely, QD lasers may exhibit both Class A and Class B dynamics depending on the carrier capture parameters as was shown in [7] by analyzing a three-variable rate equation model. Below, we consider these equations, adapted to include optical injection and examine the limit that leads to the highest damping of the ROs.

Modeling

We now turn our attention to a rate equation model of the optically injected quantum dot laser. We study the behavior of the system in different limits and show that the experimentally relevant case reproduces the experimental results very well. The first step is a 4-dimensional model of an optically injected quantum dot laser.

QD Laser Equations

Our rate equations for a QD laser subject to an injected signal consist of three equations for the complex electric field E, the occupation probability in a dot ρ, and the carrier density n in the wetting layers, scaled by the 2D QD density per layer. The free-running (no injection) case was studied in [7]. These are augmented with a term for the injected field and are given by

$$E' = \frac{1}{2}(1 + i\alpha)[-1 + g(2\rho - 1)]E + \Gamma \exp(i\Delta t), \tag{1.1}$$

$$\rho' = \eta\Big[Bn(1 - \rho) - \rho - (2\rho - 1)|E|^2\Big], \tag{1.2}$$

$$n' = \eta[J - n - 2Bn(1 - \rho)]. \tag{1.3}$$

Prime means differentiation with respect to $T \equiv t/\tau_{\text{ph}}$ where t is time and τ_{ph} is the photon lifetime (=2 ps for this work). Γ is the injection rate: it is proportional to the injection strength divided by the laser round-trip time (to give the correct units). The factor 2 in Eq. 1.3 accounts for the spin degeneracy in the quantum dot energy levels. J is the pump current per dot and α is the linewidth enhancement factor. The fixed parameters B and η are ratios of basic timescales and are defined as $B \equiv \tau\tau_{\text{cap}}^{-1}$ and $\eta \equiv \tau_{\text{ph}}\tau^{-1}$ where τ and τ_{cap} denote the carrier recombination and capture times, respectively. Typical values are $\tau = 1$ ns and $\tau_{\text{cap}} = 10$ ps which imply $B = 10^2$ and $\eta = 2 \times 10^{-3}$. The nonlinear interaction between the wetting layer and the dots is provided by the Pauli blocking factor $1 - \rho$ which leads to a significant difference between QD and QW equations. As in [10], we shall consider a value of g close to one for which a good agreement between theory and experiments is observed.

Reduction to QW Laser Equations

If we consider the limit $B \to \infty$ and keep all other parameters fixed, we obtain the conventional rate equations for an injected QW laser. This can be seen by introducing the new variable

$$N = Bn \tag{1.4}$$

into Eqs. 1.1–1.3. The equations for E, ρ, and N are then given by

$$E' = \frac{1}{2}(1 + i\alpha)[-1 + g(2\rho - 1)]E + \Gamma \exp(i\Delta t), \tag{1.5}$$

$$\rho' = \eta\Big[N(1 - \rho) - \rho - (2\rho - 1)|E|^2\Big], \tag{1.6}$$

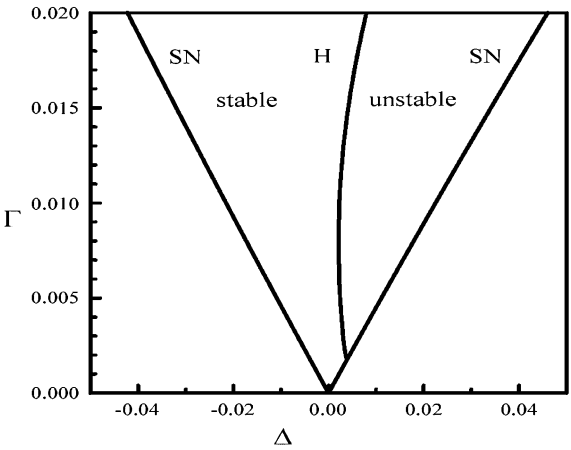

Fig. 1.12 Stability diagram in the large B limit. Steady-state locking occurs in the central region delimited by the *left* SN bifurcation line and by the Hopf (H) bifurcation line

$$N' = \eta B\left[J - B^{-1}N - 2N(1-\rho)\right]. \tag{1.7}$$

From Eqs. 1.6 and 1.7, we note that N is faster than ρ because $B \gg 1$ is multiplying the right-hand side of Eq. 1.7. This suggests the elimination of N by a quasi-steady-state approximation. Specifically, we determine N from Eq. 1.7 with $N' = 0$ and obtain

$$N = \frac{J}{2(1-\rho)} \tag{1.8}$$

as $B \to \infty$. Substituting (1.8) into Eq. 1.6, the equations for E and ρ become

$$E' = \frac{1}{2}(1+i\alpha)[-1+g(2\rho-1)]E + \Gamma\exp(i\Delta t), \tag{1.9}$$

$$\rho' = \eta\left[\frac{J}{2} - \rho - (2\rho-1)|E|^2\right]. \tag{1.10}$$

Defining

$$D = \frac{-1+g(2\rho-1)}{2}, \tag{1.11}$$

Eqs. 1.9 and 1.10 take the form

$$E' = (1+i\alpha)DE + \Gamma\exp(i\Delta t), \tag{1.12}$$

$$D' = \eta\left[P - D - (1+2D)|E|^2\right], \tag{1.13}$$

where

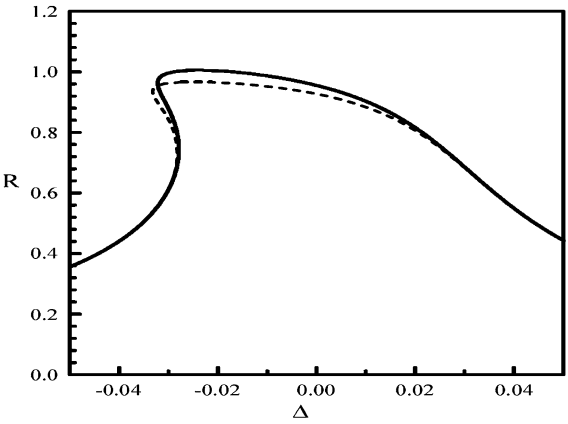

Fig. 1.13 Bifurcation diagram of the steady-state solutions. The values of the fixed parameters are those in (1.15) plus $B = 10^2$ and $\Gamma = 0.02$. The broken line is the approximation given by (1.34) and (1.35) found in the limit $\varepsilon = g - 1 \to 0$ and $B\varepsilon = O(1)$.

$$P \equiv \frac{g}{2}(J - 1 - g^{-1}) \tag{1.14}$$

is defined as the pump parameter above threshold ($J_{\text{th}} = 1 + g^{-1}$). Equations 1.12 and 1.13 are the rate equations for an optically injected QW laser [9]. A typical stability diagram is shown in Fig. 1.12.

The values of the fixed parameters α, η and g are the same for all our bifurcation studies. They are given by

$$\alpha = 1.2, \quad \eta = 2 \times 10^{-3}, \quad \text{and} \quad g = 1.02. \tag{1.15}$$

We consider $J = 1.5\, J_{\text{th}} = 2.97$ which implies from (1.14) that $P = 0.51$. In Fig. 1.12, the Hopf bifurcation line emerges from a fold-Hopf bifurcation point located on the right SN bifurcation line. As the injection rate progressively increases, the Hopf line moves slightly to the left before folding back to the right. If α is larger, the Hopf line crosses the zero detuning axis before folding back. A detailed investigation of the stability diagram in Fig. 1.12 can be found in [24].

Steady States and Stability Analysis

We next determine the basic steady-state solutions. We make the substitution $E = R\exp(i(\Delta T + \phi))$ in Eqs. 1.1–1.3 and look for solutions satisfying $R' = \phi' = \rho' = n' = 0$. Using Δ as the bifurcation parameter, the solution in parametric form (where n is the parameter) is given by

$$\rho = 1 - \frac{J - n}{2Bn}, \tag{1.16}$$

$$R^2 = \frac{1}{2[(B+1)n - J]}[Bn(J-n-2) + J - n] \geq 0, \tag{1.17}$$

$$\Delta = F\alpha \pm \sqrt{\Gamma^2 R^{-2} - F^2} \quad \text{with} \quad (\Gamma^2 R^{-2} - F^2 \geq 0) \tag{1.18}$$

where

$$F \equiv \frac{1}{2}\left[-1 + g\left(1 - \frac{J-n}{Bn}\right)\right]. \tag{1.19}$$

Note that the condition $0 \leq \rho \leq 1$ restricts the values of n to the interval

$$\frac{J}{2B+1} \leq n \leq J. \tag{1.20}$$

The steady-state solution for R is shown in Fig. 1.13. It exhibits an S-shape for negative detuning.

In the case of the solitary laser ($\Gamma = 0$), the linear stability properties of the steady states depend on an effective capture rate $B_e \equiv B(g-1)$ [7]. Because B is large and $\varepsilon \equiv g - 1$ is small, we need to specify how these quantities are related. The most interesting case that does not lead to the conventional QW laser rate equations is based on the limit

$$B = O(\varepsilon^{-1}) \text{ as } \varepsilon \to 0. \tag{1.21}$$

After introducing $g = 1 + \varepsilon$ into Eq. 1.1, the expression in brackets becomes $[-2 + 2\rho + \varepsilon(2\rho - 1)]$ and motivates the introduction of u where

$$\rho = 1 + \varepsilon u \tag{1.22}$$

to balance all terms. The expression in brackets is then proportional to ε and motivates the new time

$$s \equiv \varepsilon T \tag{1.23}$$

to balance the left- and right-hand sides of Eq. 1.1. In terms of u and s, Eqs. 1.1–1.3 become

$$E' = \frac{1}{2}(1 + i\alpha)[1 + 2u(1+\varepsilon)]E + \gamma \exp(i\delta s), \tag{1.24}$$

$$u' = \varepsilon^{-2}\eta\left[-B\varepsilon n u - 1 - \varepsilon u - (1 + 2u\varepsilon)|E|^2\right], \tag{1.25}$$

$$n' = \varepsilon^{-1}\eta[J - n + 2B\varepsilon n u] \tag{1.26}$$

where prime now means differentiation with respect to s. The new control parameters are the scaled injection strength γ and the scaled detuning δ. They are defined by

$$\gamma \equiv \varepsilon^{-1}\Gamma \text{ and } \delta \equiv \varepsilon^{-1}\Delta. \tag{1.27}$$

Adiabatic Elimination

Since $\varepsilon^{-2} \gg \varepsilon^{-1}$ as $\varepsilon \to 0$, Eqs. 1.25 and 1.26 suggest that u is faster than n. Consequently, we eliminate u by a quasi-steady-state approximation. From Eq. 1.25 with $u' = 0$, we obtain

$$u = -\frac{1+E^2}{B\varepsilon n} \tag{1.28}$$

as $\varepsilon \to 0$. Substituting (1.28) into Eqs. 1.24 and 1.26, the equations for E and n become

$$E' = \frac{1}{2}\left(1 - \frac{2(1+|E|^2)}{B\varepsilon n}\right)(1+i\alpha)E + \gamma \exp(i\delta s), \tag{1.29}$$

$$n' = \varepsilon^{-1}\eta\left[J - n - 2(1+|E|^2)\right]. \tag{1.30}$$

Introducing the decomposition $E = R\exp(i(\delta s + \phi))$ into Eqs. 1.29 and 1.30 leads to the following three equations for R, ϕ, and n

$$R' = \frac{1}{2}\left(1 - \frac{2(1+R^2)}{B\varepsilon n}\right)R + \gamma\cos(\phi), \tag{1.31}$$

$$\phi' = -\delta + \frac{1}{2}\left(1 - \frac{2(1+R^2)}{B\varepsilon n}\right)\alpha - \frac{\gamma}{R}\sin(\phi), \tag{1.32}$$

$$n' = \varepsilon^{-1}\eta\left[J - n - 2(1+R^2)\right]. \tag{1.33}$$

Steady States

The steady-state solutions can be determined analytically in the parametric form $n = n(R^2)$ and $\gamma = \gamma(R^2)$. We find

$$n = J - 2(1+R^2), \tag{1.34}$$

$$\gamma^2 = \left[F^2 + (-\delta + F\alpha)^2\right]R^2 \tag{1.35}$$

where

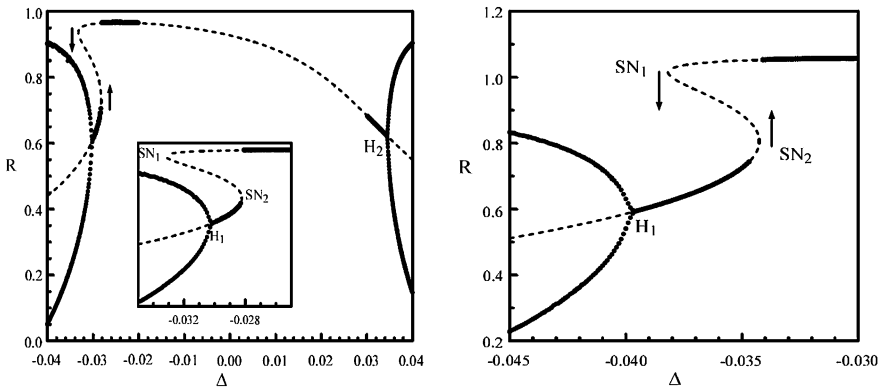

Fig. 1.14 Two bifurcation diagrams. The figure on the *left* is a bifurcation diagram of the bistability between stable steady and periodic solutions. The branch of steady-state solutions is given by Eqs. 1.34–1.36 (*broken line*). The extrema of the stable periodic solutions have been obtained by integrating Eqs. 1.31–1.33. The bistability between steady states is possible due to the Hopf bifurcation H_1 that stabilizes the lower branch of steady states. The values of the parameters are those in (1.15) plus $B = 10^2$, $J = 1.5\,J_{\text{th}} = 4.5$ and $\Gamma = 0.02$. The location of the Hopf and SN bifurcation points is in agreement with the predictions of the linearized theory (Fig. 1.15a). The figure on the *right* shows the full phase-locked bistability. The extrema of R are shown as functions of the detuning Δ. The complete S-shaped branch of steady states is shown by a *broken line*. The values of the parameters are those in (1.15) plus $B = 0.7 \times 10^2$, $J = 1.5\,J_{\text{th}} = 5.14$ and $\Gamma = 0.025$

$$F \equiv \frac{1}{2}\left(1 - \frac{2(1+R^2)}{B\varepsilon(J - 2(1+R^2))}\right). \tag{1.36}$$

The branch of steady states is shown in Fig. 1.14 by a broken line. The condition $n > 0$ implies, using (1.34), that $R^2 < (J-2)/2$. Under this condition, we note from (1.28) that $\rho < 1$ as must be the case.

Linear Stability

We next examine the stability of the steady states. From the linearized equations, we determine the following characteristic equation for the growth rate λ

$$\lambda^3 + a_1\lambda^2 + a_2\lambda + a_3 = 0 \tag{1.37}$$

where the coefficients are all expressed as functions of the steady-state intensity R^2. They are given by

$$a_1 = -G - F + \varepsilon^{-1}\eta, \tag{1.38}$$

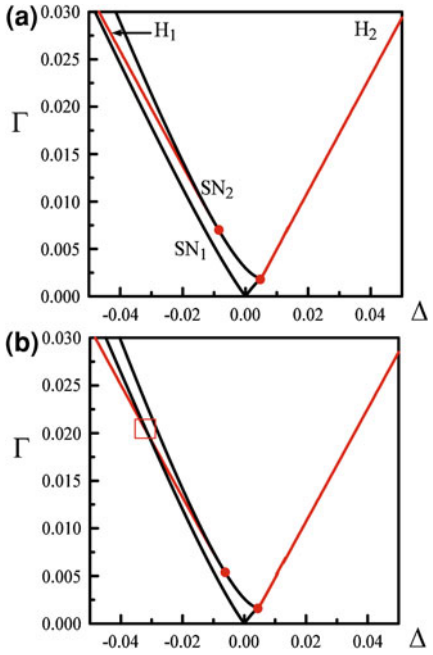

Fig. 1.15 Stability diagrams for the case $\varepsilon = g - 1 \to 0$ and $B\varepsilon = O(1)$. **a** $B = 10^2$ and $J = 1.5\,J_{\text{th}} = 4.5$; **b** $B = 0.7 \times 10^2$ and $J = 1.5\,J_{\text{th}} = 5.14$. All remaining parameters are given in (1.15). The *square* in Fig. (**b**) indicates the point where H_1 and SN_1 admit the same value of Δ. Above this point, full bistability between steady states is possible. The laser threshold of the solitary laser is determined from $J_{\text{th}} = 1 + g^{-1} + (g+1)/(B\varepsilon)$ [7]

$$\begin{aligned} a_2 =& GF + H\alpha(\delta - F\alpha) + (\delta - F\alpha)^2 \\ & - \varepsilon^{-1}\eta(G + F) + \varepsilon^{-1}\eta 4R^2 K, \end{aligned} \tag{1.39}$$

$$\begin{aligned} a_3 =& \varepsilon^{-1}\eta\left[GF + H\alpha(\delta - F\alpha) + (\delta - F\alpha)^2\right] \\ & \varepsilon^{-1}\eta 4R^2 K[\alpha(\delta - F\alpha) - F]. \end{aligned} \tag{1.40}$$

The functions $G = G(R^2)$, $H = H(R^2)$, and $K = K(R^2)$ are defined by

$$G \equiv \frac{1}{2}\left[1 - \frac{2(1+3R^2)}{B\varepsilon(J - 2(1+R^2))}\right], \tag{1.41}$$

$$H \equiv \frac{2R^2}{B\varepsilon(J - 2(1+R^2))}, \tag{1.42}$$

$$K \equiv \frac{1+R^2}{B\varepsilon(J - 2(1+R^2))^2}. \tag{1.43}$$

The Routh–Hurtwitz stability conditions for a stable steady-state require that [11]

$$a_1 a_2 - a_3 > 0, a_1 > 0 \;\text{ and }\; a_3 > 0. \tag{1.44}$$

A change of stability occurs through either an SN bifurcation or a Hopf bifurcation. The SN bifurcation point is characterized by a zero eigenvalue and satisfies the condition

$$a_3 = 0. \tag{1.45}$$

A Hopf bifurcation point is characterized by a pair of purely imaginary eigenvalues and satisfies the conditions

$$a_1 a_2 - a_3 = 0 \tag{1.46}$$

and

$$a_2 > 0. \tag{1.47}$$

Both Eqs. 1.45 and 1.46 can be solved analytically because they are quadratic expressions in the detuning δ. Specifically, we first determine δ as a function of R^2 from either Eqs. 1.45 or 1.46. We then obtain γ as a function of δ by using the steady-state Eq. 1.35. Two stability diagrams exhibiting the SN and Hopf bifurcation lines are shown in Fig. 1.15 for two different values of B. For clarity, only the Hopf bifurcation points from a stable steady state are shown ($a_1 a_2 - a_3 = 0$, $a_1 > 0$, and $a_3 > 0$).

Comparing Fig. 1.15 with the stability diagram of the conventional QW laser (Fig. 1.12), we note two distinct differences. First, a Hopf bifurcation line emerges from the SN bifurcation line at a positive detuning and moves immediately to the right. Second, an additional Hopf bifurcation emerges from the SN bifurcation line at a negative detuning. This second Hopf bifurcation allows the coexistence of either two stable steady states (bistability) or the coexistence of one stable steady state and one pulsating time-periodic regime. These predictions from the linearized theory are verified by direct simulations of Eqs. 1.31–1.33 (see Fig. 1.14).

The stability diagram in Fig. 1.15 is qualitatively similar to the experimental map. Both the experimental and analytical stability diagrams predict stable locking for a larger domain of detuning compared to a QW laser. Moreover, there are no Hopf bifurcations at low injection strengths as previously demonstrated experimentally in [14]. At higher injection strengths and for a sufficiently large positive detuning, steady-state locking occurs through a Hopf bifurcation (H_2 in Fig. 1.14) and not through an SN bifurcation. For negative detunings, there is a domain of bistability between two locked states. As previously stated, this bistability phenomenon is possible because of a Hopf bifurcation that stabilizes the lower intensity branch (H_1 in Fig. 1.14).

Because the Hopf bifurcation lines do not cross the $\Delta = 0$ axis as is the case for QW lasers [9], the injected QD laser exhibits greater stability properties. We should, however, emphasize that this results from the fact that $g - 1 \ll 1$ and $(g - 1)B = O(1)$. Other ranges of values of the parameters $g - 1$ and B are possible because of the large diversity of QD structures that are currently designed.

The stability diagram shown in Fig. 1.15 bears striking similarities with that of an optically injected Class A laser with a nonzero linewidth enhancement factor. We consider this system in the next section.

Class A Laser

Mayol et al investigated the equations for an optically injected Class A laser with a nonzero linewidth enhancement factor α in [20]. These equations are given by

$$E' = \left(\frac{A}{1+|E|^2} - 1\right)(1+i\alpha)E + \Gamma \exp(i\Delta t) \tag{1.48}$$

where A is the normalized pump parameter (laser threshold is $A = 1$) and α is the linewidth enhancement factor. The control parameters are the injection rate Γ and the detuning Δ. Introducing $E = R\exp(i(\Delta t + \phi))$ into (1.48), we obtain

$$R' = \left(\frac{A}{1+R^2} - 1\right)R + \Gamma\cos(\phi), \tag{1.49}$$

$$\phi' = -\Delta + \left(\frac{A}{1+R^2} - 1\right)\alpha - \frac{\Gamma}{R}\sin(\phi). \tag{1.50}$$

The steady-state intensity $R^2 = R^2(\Gamma)$ satisfies

$$\Gamma^2 = R^2\left\{\left(\frac{A}{1+R^2} - 1\right)^2 + \left[-\Delta + \left(\frac{A}{1+R^2} - 1\right)\alpha\right]^2\right\}. \tag{1.51}$$

From the linearized equations, we then obtain the characteristic equation for the growth rate λ

$$\lambda^2 + b_1\lambda + b_2 = 0 \tag{1.52}$$

where

$$b_1 = 2\left(1 - \frac{A}{(1+R^2)^2}\right), \tag{1.53}$$

$$\begin{aligned} b_2 = {} & \left(\frac{A}{1+R^2} - 1\right)\left[\frac{A(1-R^2)}{(1+R^2)^2} - 1\right] + \left[\Delta - \left(\frac{A}{1+R^2} - 1\right)\alpha\right]^2 \\ & + \frac{2AR^2\alpha}{(1+R^2)^2}\left[\Delta - \left(\frac{A}{1+R^2} - 1\right)\alpha\right]. \end{aligned} \tag{1.54}$$

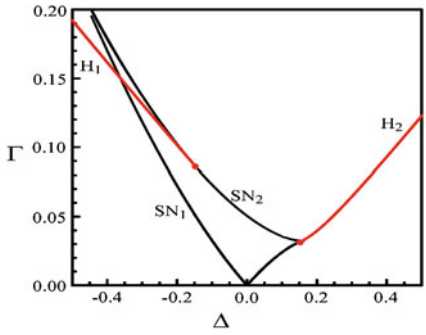

Fig. 1.16 Stability diagram for an optically injected class A laser with $\alpha = A = 1.2$.

The condition for an SN stability boundary is $b_2 = 0$ which is a quadratic equation for $\Delta - \left(\frac{A}{1+R^2} - 1\right)\alpha$. By gradually changing R^2 from zero, we first determine Δ from this quadratic equation and then evaluate Γ using Eq. 1.51 (see Fig. 1.16). The conditions for a Hopf bifurcation are $b_1 = 0$ and $b_2 > 0$. From 1.53, we find that $b_1 = 0$ if

$$R^2 = R_H^2 = \sqrt{A} - 1 \tag{1.55}$$

with $\sqrt{A} \geq 1$ and from (1.54) we find

$$b_2(R_H^2) = \left(\Delta - R_H^2\sqrt{\alpha^2+1}\right)\left(\Delta + R_H^2\sqrt{\alpha^2+1}\right). \tag{1.56}$$

We conclude that $b_2(R_H^2) > 0$ if either $\Delta < -R_H^2\sqrt{\alpha^2+1}$ or $\Delta > R_H^2\sqrt{\alpha^2+1}$. The Hopf bifurcation lines are obtained by substituting (1.55) into Eq. 1.51 and satisfy

$$\Gamma^2 = (\sqrt{A}-1)\left\{(1+\alpha^2)(\sqrt{A}-1)^2 - 2\Delta(\sqrt{A}-1)\alpha^2 + \Delta^2\right\}. \tag{1.57}$$

The critical points $\Delta = \pm R_H^2\sqrt{\alpha^2+1}$ correspond to double zero eigenvalues and are indicated by dots in Fig. 1.16.

This stability diagram bears a striking resemblance to those in Fig. 1.15 and to the experimentally obtained diagram in Fig. 1.10. This highlights again the large RO damping associated with quantum dot lasers. However, this similarity is restricted to the stability diagram and does not extend to some features such as the presence of chaos. Since the optically injected Class A laser is a 2-dimensional system it does not admit deterministic chaos while we saw that chaotic attractors do feature in the optically injected QD laser in Fig. 1.5. Thus, the optically injected QD laser occupies a sort of middle ground between weakly damped QW lasers and Class A lasers.

Conclusions

In conclusion, we have performed an experimental and theoretical study of an optically injected single-mode QD laser. Various dynamical regimes were observed experimentally. Among these were excitability for both positive and negative detuning and a number of bistabilities including most strikingly, a phase-locked bistability over a relatively large area. An experimental stability diagram was obtained and was shown to differ significantly from that of an optically injected QW laser. In particular, the Hopf bifurcation typically induced by ROs is absent from a large region of the stability diagram. Furthermore, the phase-locked bistability is not possible with weakly damped QW devices except close to threshold. A rate equation model of the system was considered and reproduced both the bistability and the qualitative features of the stability diagram. Finally, the stability diagram was shown to strongly resemble that of an optically injected Class A laser with a nonzero α-factor, further underlining the importance of the strong RO damping in QD lasers.

Acknowledgments This work was conducted under the framework of the INSPIRE programme, funded by the Irish Governments Programme for Research in Third Level Institutions, Cycle 4, National Development Plan 2007–2013 and the authors also gratefully acknowledge the support of Science Foundation Ireland (SFI) under the contract number 07/IN.1/I929 and also through the Centre for Telecommunications Value-Chain Research (CTVR), the Irish Research Council for Science, Engineering and Technology (IRCSET), the EU FP7 Marie Curie Action FP7-PEOPLE-2010-ITN through the PROPHET project, Grand No. 264687 and the Tyndall National Access Programme. The authors in Bruxelles acknowledge support of the Fonds National de la Recherche Scientifique (Belgium). The research by T. Erneux was also supported by the Air Force Office of Scientific Research (AFOSR) grant FA8655-09-1-3068.

References

1. Adler, R.: Study of locking phenomena in oscillators. Proc. IRE **34**, 351–357 (1946)
2. Arecchi, F.T., Lippi, G.L., Puccioni, G.P., Tredicce, J.R.: Deterministic chaos in laser with injected signal. Opt. Commun. **51**, 308–314 (1984)
3. Baili, G., Alouini, M., Moronvalle, C., Dolfi, D., Bretenaker, F.: Broad-bandwidth shot-noise-limited class-A operation of a monomode semiconductor fiber-based ring laser. Opt. Lett. **31**, 62–64 (2006)
4. Baili, G., Alouini, M., Dolfi, D., Bretenaker, F., Sagnes, I., Garnache, A.: Shot-noise-limited operation of a monomode high-cavity-finesse semiconductor laser for microwave photonics applications. Opt. Lett. **32**, 650–652 (2007)
5. Baili, G., Alouini, M., Malherbe, T., Dolfi, D., Sagnes, I., Bretenaker, F.: Direct observation of the class-B to class-A transition in the dynamical behavior of a semiconductor laser. Eur. Phys. Lett. **87**, 44005 (2009)
6. Bimberg, D., Grundmann, M., Ledentsov, N.N.: Quantum Dot Heterostructures. Wiley, NY (1999)
7. Erneux, T., Viktorov, E.A., Mandel, P.: Time scales and relaxation dynamics in quantum-dot lasers. Phys. Rev. A **76**, 023819 (2007)
8. Erneux, T., Viktorov, E.A., Kelleher, B., Goulding, D., Hegarty, S.P., Huyet, G.: Optically injected quantum dot lasers. Opt. Lett. **35**, 937–939 (2010)

9. Erneux, T., Glorieux, P.: Laser Dynamics. Cambridge University Press, Cambridge (2010)
10. Goulding, D., Hegarty, S.P., Rasskazov, O., Melnik, S., Hartnett, M., Greene, G., McInerney, J.G., Rachinskii, D., Huyet, G.: Excitability in a quantum dot semiconductor laser with optical injection. Phys. Rev. Lett. **98**, 153903 (2007)
11. Gradshteyn, I.S., Ryzhik, I.M.: Routh-Hurwitz Theorem. In: Tables of Integrals, Series, and Products. 6th edn. Academic Press, San Diego (2000)
12. Hegarty, S.P., Goulding, D., Kelleher, B., Huyet, G., Todaro, M.T., Salhi, A., Passaseo, A., De Vittorio, M.: Phase-locked mutually coupled 1.3 μm quantum-dot lasers. Opt. Lett. **32**, 3245–3247 (2007)
13. Hohl, A., van der Linden, H.J.C., Roy, R., Goldsztein, G., Broner, F., Strogatz, S.H.: Scaling laws for dynamical hysteresis in a multidimensional laser system. Phys. Rev. Lett. **74**, 2220–2223 (1995)
14. Kelleher, B., Goulding, D., Hegarty, S.P., Huyet, G., Ding-Yi, C., Martinez, A., Lemaître, A., Ramdane, A., Fischer, M., Gerschütz, F., Koeth, J.: Excitable phase slips in an injection-locked single-mode quantum-dot laser. Opt. Lett. **34**, 40–42 (2009)
15. Kelleher, B., Bonatto, C., Skoda, P., Hegarty, S.P., Huyet, G.: Excitation regeneration in delay-coupled oscillators. Phys. Rev. E **81**, 036204 (2010)
16. Kelleher, B., Bonatto, C., Huyet, G., Hegarty, S.P.: Excitability in optically injected semiconductor lasers: contrasting quantum-well- and quantum-dot-based devices. Phys. Rev. E **83**, 026207 (2011)
17. Kuntz, M., Ledentsov, N.N., Bimberg, D., Kovsh, A.R., Ustinov, V.M., Zhukov, A.E., Shernyakov, Y.M.: Spectrotemporal response of 1.3 μm quantum-dot lasers. Appl. Phys. Lett. **81**, 3846–3848 (2002)
18. Lüdge, K., Bormann, M.J.P., Malic, E., Hövel, P., Kuntz, M., Bimberg, D., Knorr, A., Schöll, E.: Turn-on dynamics and modulation response in semiconductor quantum dot lasers. Phys. Rev. B **78**, 035316 (2008)
19. Martinez, A., Lemaître, A., Merghem, K., Ferlazzo, L., Dupuis, C., Ramdane, A., Provost, J.G., Dagens, B., Le Gouezigou, O., Gauthier-Lafaye, O.: Static and dynamic measurements of the α-factor of five-quantum-dot-layer single-mode lasers emitting at 1.3 μm on GaAs. Appl. Phys. Lett. **86**, 211115 (2005)
20. Mayol, C., Toral, R., Mirasso, C.R., Natiello, M.A.: Class-A lasers with injected signal: bifurcation set and Lyapunov-potential function. Phys. Rev. A **66**, 013808 (2002)
21. O'Brien, D., Hegarty, S.P., Huyet, G., Uskov, A.V.: Sensitivity of quantum-dot semiconductor lasers to optical feedback. Opt. Lett. **29**, 1072–1074 (2004)
22. Simpson, T.B.: Mapping the nonlinear dynamics of a distributed feedback semiconductor laser subject to external optical injection. Opt. Commun. **215**, 135–151 (2003)
23. Wieczorek, S., Krauskopf, B., Lenstra, D.: Multipulse excitability in a semiconductor laser with optical injection. Phys. Rev. Lett. **88**, 063901 (2002)
24. Wieczorek, S., Krauskopf, B., Simpson, T.B., Lenstra, D.: The dynamical complexity of optically injected semiconductor lasers. Phys. Rep. **416**, 1–128 (2005)